

Article

Not peer-reviewed version

---

# Response of the bGeigie Nano and CzechRad Monitors to Secondary Cosmic Radiation

---

[Petr Kuča](#), Jan Helebrant, [Peter Bossew](#)\*

Posted Date: 7 November 2024

doi: 10.20944/preprints202411.0463.v1

Keywords: bGeigie Nano; CzechRad; G-M detector; secondary cosmic radiation



Preprints.org is a free multidisciplinary platform providing preprint service that is dedicated to making early versions of research outputs permanently available and citable. Preprints posted at Preprints.org appear in Web of Science, Crossref, Google Scholar, Scilit, Europe PMC.

Copyright: This open access article is published under a Creative Commons CC BY 4.0 license, which permit the free download, distribution, and reuse, provided that the author and preprint are cited in any reuse.

*Article*

# Response of the bGeigie Nano and CzechRad Monitors to Secondary Cosmic Radiation

Petr Kuča<sup>1</sup>, Jan Helebrant<sup>1</sup> and Peter Bossew<sup>2,\*</sup>

<sup>1</sup> National Radiation Protection Institute (SÚRO), Praha, Czech Republic

<sup>2</sup> Hiroasaki University, Japan

\* Correspondence: peter.bossew@reflex.at

**Abstract:** Ambient dose rate surveying has the objective, in most cases, to quantify terrestrial radiation levels. This is true in particular for Citizen Monitoring projects. Readings of detectors, which do not provide spectrally resolved information, such as G-M counters, are the sum of contributions from different sources, including cosmic radiation. To estimate the terrestrial component, one has to subtract the remaining ones. In this paper, we investigate the cosmic response of two particular monitors, the bGeigie Nano which has been used extensively in the Safecast Citizen Monitoring project and its upgraded version, the new CzechRad which uses the same G-M detector, and show how the local contribution of cosmic radiation can be estimated.

**Keywords:** bGeigie Nano; CzechRad; G-M detector; secondary cosmic radiation

## 1. Introduction

Citizen Science (CS) means scientific research conducted by citizens who are not professional scientists. Their involvement can range between participating to different degree in defined projects and setting up entire projects. Citizen monitoring (CM), as a discipline in CS, focuses on data acquisition and is a potentially extremely powerful way to monitor and survey environmental quality regarding pollution due to anthropogenic routine or accidental activity, or the natural background. For a large compendium of CS across fields of science, see [1] and the very comprehensive Wikipedia entry about CS, [https://en.wikipedia.org/wiki/Citizen\\_science](https://en.wikipedia.org/wiki/Citizen_science).

A very successful CM project is Safecast [2] (<https://blog.safecast.org/>). Among other, this platform enabled creating a world-wide map of ambient dose rate (ADR) through contributions of numerous citizens, still expanding, who submit data which they have acquired using a standard monitor (Currently, October 2024, the map is not active). Data and methodology are openly accessible. The project has been founded shortly after the Fukushima accident 2011 in Japan motivated by the perceived mistrust in official information policy, and soon spread world-wide. Several thousand citizens contribute as volunteers, carrying detectors and sending data to Safecast.org, where they are presented in a freely accessible map. The project uses a standard device called bGeigie Nano (based on a G-M detector) which is the subject of investigation in this paper, but in principle also other monitors of similar type can be used.

Among the benefits of CM is its ability to generate large amounts of data, its contribution to democratization of science and its educative potential. On the other hand, CM is mostly performed by people who are no metrological professionals. This causes QA problems, in particular related to the notions of representativeness, observation protocol and interpretability of results.

This paper aims to one particular aspect of interpretability. Most dose rate monitors, especially those based on G-M detectors, do not provide spectral information of incident radiation. The reading of the instrument represents the sum of several components, namely, terrestrial radiation, cosmic radiation, airborne radiation and internal background. Usually in areal monitoring, one is interested only in the geographical variability of terrestrial radiation; in this case, one step in the task of data interpretation consists in trying to subtract the other components.

If no independent measurement of these components is available, which is the most common case, one has to estimate them from other information. Here, we concentrate on estimation of the cosmic component, but also discuss internal background and contribution of airborne radon progeny, because they play a role in assessing the response of the device to cosmic radiation.

In the rather long methods section 2, we start with some basics on cosmic radiation (section 2.1), followed by discussion of the response of G-M detectors to cosmic radiation in general (section 2.2) and factors that influence the intensity of cosmic radiation (sections 2.3), followed by description of the bGeigie Nano and CzechRad monitors (section 2.4). Next in section 2.5, components of radiation registered by the monitor are discussed in more detail. Finally, in section 2.6. we propose two methods for assessing cosmic response. Results from application of these methods are presented in section 3.

This paper builds on practical experience of the authors in working with the bGeigie Nano and CzechRad devices and deepens information which in lesser detail has been incorporated in previous publications, such as [3–9].

## 2. Materials and Methods

### 2.1. Secondary Cosmic Radiation

Cosmic rays originate from galactic and intergalactic space and to smaller extent from the sun. They consist mainly of protons and a small fraction of heavier nuclei. Interaction with the atmosphere results in secondary cosmic radiation (SCR), mainly composed of muons, neutrons and a small contribution of pions, electrons and photons. Muons, electrons and charged pions form the charged particle fraction of SCR, whereas the uncharged fraction is composed of neutrons, photons and neutral pions. Here we are especially interested in the muon component, called “hard” component because of the high energy of muons (between 1 and 20 GeV; UNSCEAR 2000 [10], annex B, p.86). The composition of SCR is strongly variable with altitude, see e.g. [11], Figure 30, reproduced in [10] UNSCEAR 2000, Annex B, p.85, which has consequences for the response characteristic of radiation monitors (see below). The intensity of SCR depends on several factors:

- Mass of air above the measurement point, related to air pressure, in turn mainly controlled by altitude above sea level (a.s.l.) plus variations caused by meteorological variability. For estimating local SCR dose rate, usually altitude a.s.l. is taken as an approximate predictor. [12] gives the figure  $\Delta\text{ADR}/\text{ADR} \approx -0.01564 \Delta p[\text{kPa}]$  for muons. For variations of 10 kPa (100 hPa; standard air pressure at sea level is 1013 hPa) due to weather variation, one thus finds about 15.6% ADR variation.
- Geomagnetic latitude: The intensity of SCR at certain altitude depends on its diversion by the geomagnetic field (measured by the geographically variable so-called cut-off rigidity; e.g. [13]; Figure 2). Geomagnetic and geographical latitudes coincide only very approximately; lowest SCR intensity is found in the equatorial region, highest at high latitudes. Since the magnetic axis (the theoretical line between magnetic poles) does not coincide with the geographical axis and moreover does not pass through the centre of the Earth, the geomagnetic field appears distorted compared to the geometry of the globe (e.g., <https://geomag.bgs.ac.uk/education/earthmag.html>). The SCR intensity difference between equator and 60° N is about 10% at ground level ([14]), higher for higher altitudes. From figures given in [15] (Table 2), one finds that intensity in terms of dose equivalent rate is 6% and 10% higher at 55°N than 43°N at sea level and at 3 km a.s.l., respectively, during solar minimum (2% and 6%, respectively, during solar maximum).
- Solar activity: Higher solar activity and resulting solar wind leads to repulsion of galactic cosmic rays. SCR intensity therefore follows the about 11-year solar activity cycle (which is itself modulated by longer-term cycles and overlaid by irregular variability components). During solar minima, SCR intensity at ground altitude can be up to 10% higher than during solar maxima. An irregular component is added by so-called Forbush events, which is a sudden and short-term (lasting about a week) decrease of SCR due to solar coronal mass ejection. The last solar activity minimum occurred about 2019/2020 [16], the last activity maximum in 2024, expected to extend to-2025.

- Seasonal effect: According to [12,17], “owing to temperature changes in the upper layer of the atmosphere, the muon production rises in summer and, thus, the mean path [length] to ground level increases”. Due to short lifetime of muons, a longer journey to the ground in summer results in fewer muons reaching the ground. The variation amounts to about 3%. (The result is valid for Northern temperate latitude.)

[12] concludes that the contributions of the latter two effects to uncertainty of ADR measurement is 6.9 nSv/h at ground level, unless SCR is actually known through particular measurement. To make the matter even more complicated, [18] note that G-M probes as used in the German ADR network “seem to change their response to SCR with increasing altitude” (because of changing composition of the SCR, the authors presume).

A European map of dose due to SCR is shown in [19] and in the European Atlas of Natural Radiation, [20], together with physical background information. [21] calculated doses due to cosmic radiation for the world population. Useful information also in ICRU (2010) [22].

## 2.2. Response of G-M Detectors to Cosmic Radiation

### 2.2.1. Response to Muons

ADR detectors respond to SCR characteristically to the type of device. Usually, this is assessed by measuring during airplane or balloon ascents above sea or on sufficiently large lakes (see section 3.2) in different altitudes. For some discussion of cosmic response, see [23] (section 2.2.3) and references there.

Anisotropy in response to secondary cosmic radiation has been discussed by [24] (pp. 20-22). For the muonic component of SCR (which is the only one relevant in the context of G-M counters) follows from that report (rearranging from its eqs. 3.1-3 and 3.1-4), that for cylindrical detectors with effective radius and length  $R$  and  $L$ , respectively, the ratio of response  $R_{\text{Resp}}$  (axis horizontal : axis vertical) is approximately

$$R_{\text{Resp}} \approx (1.583 + Q)/(1 + 2Q),$$

with  $Q := R/L$  (shape factor). Note that “axis horizontal” and “axis vertical” are equal to the “vertical position” and the “horizontal position” in the terminology of this paper. We do not know whether the thin window of the pancake detector used in the bGeigie Nano and the CzechRad affects this reasoning.

The bGeigie Nano and CzechRad have  $Q=1.756$  and consequently,  $R_{\text{Resp}} = 0.740$ , saying that in vertical position (axis horizontal), the detector is 0.740 as sensitive to cosmic muons as in horizontal position (axis vertical). The same considerations seem to apply for other charged particles, i.e. electrons and protons. In horizontal position, there is very little difference, if at all, between the positions of the thin window pointing upwards or downwards. (Therefore, the vertical position is recommended as standard, because it reduces the influence of the SCR on the total reading.) Field measurements above a lake performed in autumn 2024 gave a preliminary empirical value  $R_{\text{Resp}} = 0.708 \pm 0.010$ . Further experiments are planned, details of the experiments and results will be published elsewhere. We do not know how precisely the Spiers model [24] is applicable to the particular geometry and architecture (different materials, window) of the detector used in the bGeigie Nano and the CzechRad.

### 2.2.2. Response of G-M Detectors to Neutrons

Neutrons, also part of cosmic radiation, contribute very little to GM signals, although they are an important part of total cosmic ray dose. The sensitivity to neutrons relative to photons is quantified by the so-called  $k_n$  value, which is in the order of 1% for the typical energies of cosmic neutrons in low altitudes, whose spectral peaks are at 1 and 10 MeV. References include [25–29].

## 2.3. Dependence of Secondary Radiation on External Factors

### 2.3.1. Altitude Dependence



Although from a rigid physical point of view, SCR intensity depends on the air mass above (hence on air pressure), approximate formulae of altitude dependence have been proposed, which make calculation simpler. In particular if survey data are evaluated retrospectively, air pressure is not available. Usual pressure variation due to meteorological difference induce a variability of SCR of several percent, see section 2.1, first bullet.

The most quoted formula for the charged particle component  $Z$  ( $H^*(10)$ , nSv/h), mainly muons, which is of interest here, comes from Bouville and Lowder (1988) [14] after [15], also quoted in UNSCEAR 2008 [10], annex B, p.233ff and [20], p.161 (for the annual effective dose; here recalculated nSv/h ADER, assuming that effective dose is about equal to  $H^*(10)$ ):

$$Z = 6.542 \exp(-1.649 h) + 25.349 \exp(0.4528 h), \quad (1)$$

$h$  in km a.s.l.,  $Z$  in  $H^*(10)$  nSv/h. It has been derived from measurements in 1965 (near solar maximum, i.e. SCR minimum) at 50°N geomagnetic latitude. Apparently an ionization chamber has been used [30] which responds differently from a GM-counter.

For the German GS-05 monitor, used in the Early Warning Network IMIS ([www.bfs.de/EN/topics/ion/accident-management/bfs/environment/imis.html](http://www.bfs.de/EN/topics/ion/accident-management/bfs/environment/imis.html)), the following mean altitude dependence has been estimated (G-M tube vertical, geometry very different from bGeigie Nano and CzechRad):

$$Z = 41.71 + 1.131 \cdot 10^{-2} h - 2.08 \cdot 10^{-6} h^2 + 1.9 \cdot 10^{-9} h^3, \quad h \text{ in meters.} \quad (2)$$

The approximate altitude effect for the charged component is shown in Figure 1. It is calculated from data which underlay Figures 2 and 3 in [23]. BL1988 refers to [14], Wiss05 to measurements in [17] using the GS05 monitor of the German ADR network, GS05 the above formula derived from data of this monitor and Sto01, a simplified formula for the same purpose (both only internally published; internal background, section 2.4.1, subtracted). For low altitudes below about 2.5 km a.s.l., the values coincide rather well.

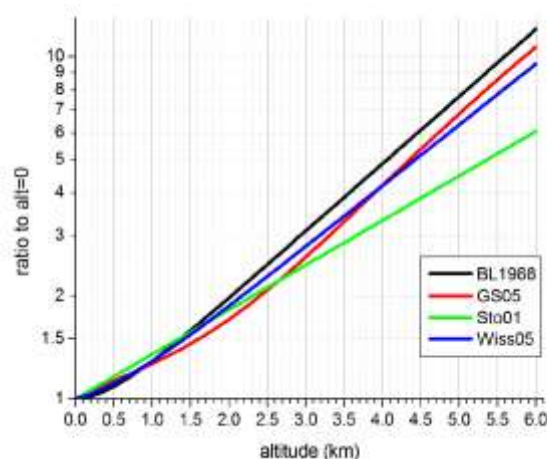


**Figure 1.** Approximate altitude variation of SCR intensity, charged component. For legend codes see text.



**Figure 2.** LND 7317 Pancake GM detector. Picture from the manufacturer's web page.

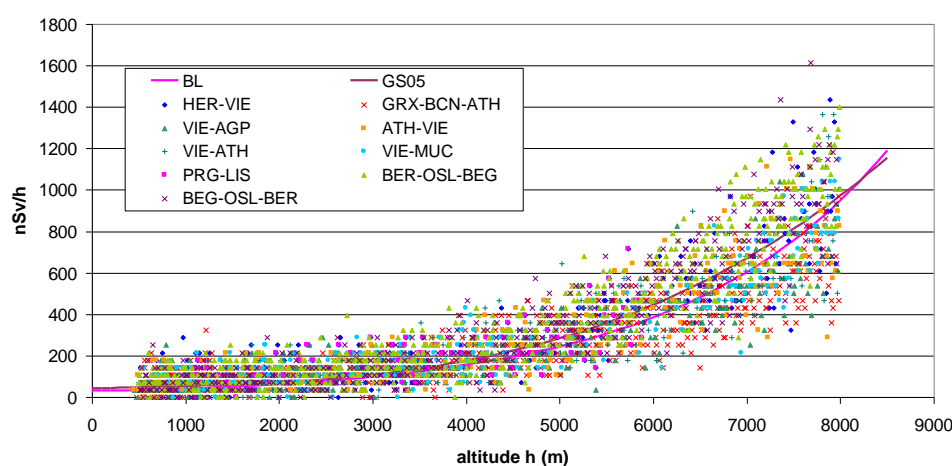


**Figure 3.** Dependence of dose rate recorded with bGeigie Nano detectors on flight altitude above sea level (GPS data). Flights according to Table 1. Theoretical values from the Bouville-Lowder formula (BL; eq. 1) and the GS05 are added (section 2.3.1; eq. 2).

### 2.3.2. Dependence on Solar Activity

Since solar activity modulates cosmic particle flux, one can expect SCR intensity following the same pattern. However, according to UNSCEAR 1982 [10] (graph in annex B, p.85), the effect is very small at ground level. On the other hand, it is notable in aircraft cruise altitude according to UNSCEAR 2000 [10] (graph in annex B, p.88). At sea level, variation in dose rate has been estimated to be higher, namely about 10 % over the 11-year solar cycle [12,14].

[31] investigated the variation of SCR at ground level between 2002 and 2015. The database includes selected stations of the EURDEP system in the far North of Europe or high in the mountains. For each year, the minimum was chosen which coincides with thickest snow cover (strongest shielding of terrestrial radiation). The ensemble mean  $\bar{Y}$ , standardized to the 2012 value, was fitted with a sinusoid,

$$y = A \sin[(2\pi/11)(t-\varphi)], \quad (3)$$

$t$  in decimal years,  $A = 0.037 \pm 0.016$  (i.e. an amplitude 3.7%), phase  $\varphi = 2004.96$ . This empirical model is significant,  $p < 0.01$ , but possibly not optimal.  $\bar{Y}$  is positively correlated with neutron flux (Oulo data, <https://cosmicrays.oulu.fi/>;  $r^2 = 0.52$ ) and  $^7\text{Be}$  concentration in air (REM-db sparse network,

[32],  $r^2=0.25$ ), negatively correlated with sunspot number (<https://www.sidc.be/silso/datafiles>;  $r^2=0.44$ ).

### 2.3.3. Dependence on Geographical Latitude

As explained above, the relevant latitude is the geomagnetic, but not the geographical one. However the geomagnetic latitude is rarely known in practice, therefore the geographical one is used as an approximation. The geomagnetic latitude of a location can be calculated from observation data. But geomagnetic coordinates move considerably fast against the geographical grid, so that using geomagnetic coordinates is impractical. In the internet, several facilities for calculating geomagnetic from geographical coordinates for a given time are available, such as [33] and [34]. The dose rate is about 10 % lower at the geomagnetic equator than at high latitudes (UNSCEAR 2008, [10] Annex B; [14]).

### 2.4. The bGeigie Nano and CzechRad Monitors

The bGeigie Nano monitor has been developed by the Safecast team since 2011 in several stages. The current version has been the standard instrument for about 7 years. In the following years, it has also been adopted as standard device in the Czech Republic in a project “RAMESIS” of the national radiation protection authority [35–38] aimed to equip citizens, schools and the like with radiation monitors and relatively easy to use free QGIS mapping software [39] as part of environmental education. Similar attempts have been on the way in Slovakia, [40].

In the Czech Republic, the device has been replaced by an upgraded version called CzechRad since 2023, but using the same detector and following the same philosophy, [41]. A better GPS module is used and other minor technical modifications have been applied.

The bGeigie Nano has been subjected to QA in dosimetric laboratories, and its behaviour in a well controlled metrological environment is moderately well documented, [42,43].

According to <https://github.com/Safecast/bGeigieNanoKit/wiki/Specifications>, the GM detector is a “LND Inc. Type 7317 Pancake Halogen-Quenched Geiger-Mueller (GM) tube, 2”; Effective diameter 1.75” (45 mm); Mica window density 1.5-2.0 mg/cm<sup>2</sup>. Capable of detecting Alpha, Beta and Gamma radiation. It comes with Medcom iRover controller and HV (high voltage) supply. Its accuracy is  $\pm 10\%$  typical,  $\pm 15\%$  maximum, the allowable temperature range,  $-20^\circ$  to  $+50^\circ$  C.” More information is given by the manufacturer, [www.lndinc.com/products/geiger-mueller-tubes/7317](http://www.lndinc.com/products/geiger-mueller-tubes/7317) from where also the picture is taken (Figure 2).

Unfortunately, calibration of the bGeigie Nano is not very well documented. The only document available to us is [42]. In an experiment performed at Jülich Research Centre (Germany), a bGeigie Nano (complete in its case) was positioned in a <sup>137</sup>Cs gamma beam, once facing the beam (“horizontal position”), then perpendicular to it (“vertical”). Different true dose rates were applied. For the lowest (with 10  $\mu$ Sv/h still high), the calibration factors were 361 and 238 cpm/( $\mu$ Sv/h) for horizontal and vertical position, respectively (calculated from the figures given there). It is not clear whether the  $\mu$ Sv/h denote ambient dose equivalent rate (ADER),  $H^*(10)$ , as it should be in Europe. But since the described experiment has been performed in Jülich (Germany), it can be plausibly assumed. (The generic quantity is denoted ADR, while the values denote ADER because of the calibration to it; similar to the quantity “length”, measured in units “meters”.)

The ratio of sensitivities between horizontal and vertical positions equals 1.60 (for low doses), i.e. the detector is 60% more sensitive in the position facing the beam, than perpendicular to it. However it must be emphasized that this is true only for the experimental setup of the laboratory using a narrow beam, but not for field conditions. In these, the detector is exposed to an area source, namely the ground containing gamma radiating radionuclides, above which it is positioned (plus cosmic rays and Rn progeny, to be discussed separately).

In <https://github.com/Safecast/bGeigieNanoKit/wiki/Specifications>, a calibration factor 334 cpm/( $\mu$ Sv/h), corresponding 35.9 (nSv/h)/(counts per 5s), is quoted for ambient radiation, i.e. from area sources in contrast to point sources. This is the factor which is implemented in the bGeigie Nano software and which is used in the Safecast map. We do not know how this factor has been determined,

to which detector orientation it refers and whether it denotes ADER. According to our own investigations, variability (1 SD) between exemplars of the device is about 4%. Calibration by the Safecast team was carried out with a  $^{137}\text{Cs}$  source, thus it refers to 662 keV. This made sense because the bGeigie Nano was initially conceived for surveying contamination in the region affected by Fukushima fallout. Today detectors for environmental surveys are preferably calibrated with  $^{226}\text{Ra}$  whose spectrum better resembles ambient gamma ray spectra. Also the CzechRad was calibrated with  $^{137}\text{Cs}$ . However, since the weighted mean energy of typical ambient spectra is close to the one of  $^{137}\text{Cs}$ , these difference are not very important.

Regarding gamma rays, impulses recorded by a G-M counter result mainly from interaction of photons with the detector case. Muons interact also directly with the gas filling of the detector. Electrons are largely absorbed by the detector case. The exact physical processes which lead to a certain response of the detector to incident radiation are quite complicated.

Counting cycles are 5 s, which for typical mean ambient radiation levels (1-4 counts/5s) leads to rather high uncertainty. Therefore, sliding means over 12 cycles, i.e. 1 minute are used in the map but also the counts / 5s are stored on the SD card. These were used in our evaluations. Again according to our investigations, the internal clocks of the bGeigie Nanos are a bit inaccurate and the counting cycle deviate slightly from 5 s, but differently for each exemplar so far investigated. The mean cycle length of 14 analyzed exemplars of bGeigie Nano is  $5.015 \pm 0.009$  s (1 SD), or a deviation of 0.28% from the nominal 5 s. This effect, although very small compared to other uncertainty components and irrelevant in practical usage, adds to sample deviation of measured sensitivity between bGeigie Nano exemplars. It also makes comparison of parallel operating monitors difficult because after some time they are out of pace. The CzechRad monitors seem to have a more accurate timer. Further, the detectors tend to produce spurious count numbers occasionally, that is, counts within one separated cycle which cannot be explained by Poisson statistics or very short external pulses. The occurrence frequency is different between detectors [5].

## 2.5. Components of Ambient Dose Rate Readings

### 2.5.1. Internal Background

Even without external radiation hitting the detector, it will record pulses. Their sources are traces of radionuclides within the detector material and electronic noise. The most common way to determine this internal background (also called intrinsic BG or zero effect) is measurement within lead shields (usually coated with thin layers of Cd and Cu to shield  $K_{\alpha}$  fluorescence rays from Pb and Fe) located in deep underground salt mines. Salt contains practically no natural radionuclides; remaining gamma radiation is almost completely shielded by the lead. The depth below surface shields from most of cosmic muons. World-wide, several underground laboratories of the kind exist. The method can be applied for the bGeigie Nano only by turning it on while a GPS signal is available; it will continue recording if the signal disappears. If it is turned on in absence of a GPS signal it will measure but not record. The feature complicates its use underground to some extent. This issue has been solved better for the CzechRad which creates an extra file if no GPS is available.

### 2.5.2. Measurement in Absence of the Terrestrial Component

An alternative is measurement in situations without terrestrial radiation, when only BG and cosmic components are present that contribute to the count rate. Experiments have to be performed to separate these components. Some experiments are described in this section. For a more thorough discussion of ADR components, see e.g. [23] and references there.

Several sets of bGeigie Nano and CzechRad data measured above water were analysed, see section 2.6.2. If the water body (lake, sea, large river) is deep enough, practically at least 3 m, and the measurement is performed far away from the shore, practically at least 100 m, the ADR is composed of

$$\begin{aligned} \text{ADR} &= \text{internal background (BG)} \\ &+ \text{cosmic dose rate (DR)} \end{aligned}$$



- + dose rate produced by radionuclides contained in the boat plus (in some cases) persons, possibly attenuated by shielding
- + DR from radionuclides in water
- + DR from radionuclides in the air.

The water component can be assumed negligible. Contribution of cosmogenic radionuclides suspended in air deposited on the ground (mainly <sup>7</sup>Be and <sup>22</sup>Na) is below 1 nSv/h, [23] and references there.

2.5.3. Radon Progeny

The air component, due to radon progeny (mainly <sup>214</sup>Pb and <sup>214</sup>Bi), depends on the proximity of solid ground that exhales Rn. Over sea, the air component is practically zero (e.g. [44] report ~10 μBq/m<sup>3</sup> over the equatorial Pacific Ocean), while on lakes it can amount to a few up to a few 10 nSv/h, depending on the geological nature of the surrounding land (hence Rn exhalation from the ground) and meteorological conditions. Factors of the latter are height of the atmospheric mixing layer, wind speed and soil humidity which affects Rn transport in the ground and thus the exhalation rate. Typical in-land <sup>222</sup>Rn concentration is 10 Bq/m<sup>3</sup> (ADER about 3 nSv/h), while over granite and ground with high gas permeability and thus high Rn exhalation, 20 Bq/m<sup>3</sup> (ADER 6 nSv/h) and higher are possible. Locally, 100 Bq/m<sup>3</sup> (ADER ≈30 nSv/h) have been reported. The values can be assumed representative for geographically similar areas. For a literature review on outdoor Rn surveys, see [45].

Dose conversion factors (DCF) of <sup>214</sup>Pb and <sup>214</sup>Bi for submersion in a semi-infinite air volume are, according ICRP 144 [46] (p.105; H\*(10)): 0.416 and 0.076 (nSv/h)/(Bq/m<sup>3</sup>), respectively, or 0.492 as sum. EPA (2019), [47], p. 211, for adults: 0.26 and 0.04, respectively, or sum 0.30; Previous sources are [48]: 0.5 for EEC; DOE (1988) [49]: effective dose (recalculated from obsolete units): 0.25 and 0.029, respectively or sum 0.28; [50], p.196: 0.236 and 0.043, respectively, or sum=0.33. Here, we propose using 0.5. With outdoor equilibrium factor F=0.6 (UNSCEAR 2000, [10] annex B, §213, p.203), 10 Bq/m<sup>3</sup> of <sup>222</sup>Rn yield 10 × 0.6 × 0.5 = 3 (nSv/h)/(10 Bq/m<sup>3</sup>). [51] found F = 0.34 to 0.62, mean 0.48 in a German survey; an overview of equilibrium factors: [52].) However we think that uncertainties of DCF and F are of minor importance compared to estimation of local Rn concentration.

2.6. Determination of the Internal Background and Cosmic Response

2.6.1. Method I: Aircraft Ascent and Descent

bGeigie Nano monitors were carried on several airplane journeys within Europe. The routes are shown in Table 1. In all cases the monitors were in vertical orientation (axis of the detector horizontal) and positioned close to a window. The journeys took place between autumn 2022 and summer 2024, i.e. close to the solar activity maximum (late 2024 - early 2025) [16], which means low intensity of SCR. Radiation by aircraft components, passengers and cargo, as well as attenuation by aircraft components is unknown and has not been considered. The same applies to gamma radiation from radon progeny in the outside atmosphere, but this component is probably very low, below 1 nSv/h we assume. Above 0.5 km above ground, the terrestrial gamma component can be neglected.

It should be emphasized that measured dose rates do not represent the doses received by persons in the airplane, because the monitors are not calibrated for cosmic radiation. This applies in particular to higher altitude, since the composition changes with altitude.

Table 1. Dose rate measurements during flights.

Flights	Dates	monitor #	approximate cruising altitudes (km)
Berlin (BER) ↔ Oslo (OSL) ↔ Bergen (BEG)	September 2022	3273	9.32; 9.51; 10.18 - 10.30; 11.14 - 12
Prague (PRG) - Lisbon (LIS)	October 2022	3281	GPS failed at cruising alt.

Athens (ATH) ↔ Vienna (VIE)	May-June 2023	3273	10.80 - 10.87; 10.58; 11.83 - 11.93
VIE - Munich (MUC)	November 2023	3273	9.1 - 9.2
VIE - Malaga (AGP)	June 2024	3273	10.68 - 10.7; 11 - 11.3; 11.68 - 11.74
Granada (GRX) - Barcelona (BCN) - ATH	June 2024	3273	11.4 - 11.5; 11.78 - 11.85
Heraklion (HER) - VIE	July 2024	3273	9.38 ; 11.24 - 11.53

In addition, to investigate the latitude effect, we evaluated the measured dose rate by GPS latitude. This was done separately in ascent / descent and in cruising phases of flights. Cruising altitude is typically 10 - 13 km. To compare the values between flights, they were normalized as

$$Y_{norm} := Y/Y_0, \quad Y_0 \text{ according to the third order polynomial of Figure 4.} \tag{4}$$

The normalized response refers to the vertical position of the monitor. All data for high solar activity.

2.6.2. Method II: Measurement Above Water Bodies in Different Altitudes

Let  $Y(\text{raw})$  the measured ADR values (ADER in nSv/h). ‘BG’ denotes the internal background (which shall be estimated),  $R_n$ , the ADR component caused by gamma rays from  $R_n$  progeny, ‘cosm × f’ the adjusted cosmic component (see below) and ‘other’ any other possibly contributing components, such as persons present during measurement (a very small effect, if at all), remaining terrestrial gamma radiation and gamma radiation of the platform on which the experiment takes places.

Then, the model reads:

$$Y(\text{raw}) = BG + R_n + \text{cosm} \times f + \text{other}. \tag{5a}$$

If sufficiently many measurements  $Y(\text{raw})$  are available and ‘ $R_n$ ’ and ‘other’ can be approximately guessed, ‘BG’ and the cosmic response can be estimated by regression.

Assumptions:

- All measurements were performed with detectors which have the same BG. This is not exactly true in reality, but one has to live with this uncertainty, about 10%.
- Outdoor radon concentration can be guessed approximately from experiences about mean  $R_n$  concentration in different geographical regions. The value is subject to meteorological variability (specifically, height of the atmospheric mixing layer), on which we have no control, but which we can guess to vary by factors (0.1, 5) and more. Many studies have been conducted about temporal variability of outdoor  $R_n$  concentration. References include UNSCEAR (1988) [10] (Annex A, §85ff), [53–68]. It would be worthwhile to further evaluate literature to refine estimation of the ADR component due to  $R_n$  in dependence on measurement season and time.
- For the cosmic component we use the estimated value of the GS-05 G-M counter in vertical position (used in the German Early Warning Network) in Northern temperate latitude according to the formula given in [3], eq. 2, and the Bouville-Lowder formula (eq. 1). Factors  $f$  are applied: for low latitudes, cosmic dose rate is assumed 10% lower; if the value  $Y(\text{raw})$  by bGeigie has been measured with detector horizontal (axis vertical),  $f=1.412$  (see section 2.3) (no distinction between window facing up or down made at this stage). Uncertainty of  $\text{cosm} \times f$  is probably 10% at most.

The regression model can then be rewritten:

$$Y(\text{raw}) - R_n - \text{other} =: Y = BG + b \times (\text{cosm} \times f). \tag{5b}$$

$b$  denotes the response of the bGeigie relative to GS-05. “other” denotes the dose rate component from nearby objects such as a boat or a bridge on which the experiment is performed or by the presence of persons (who contain gamma radiating  $^{40}\text{K}$ ).

The quantities to be estimated are hence BG and  $b$ .  $Y$  is the dependent and  $(\text{cosm} \times f)$  the independent variable.

3. Results and Discussion

We report two types of experiments: (1) Evaluation of the readings of bGeigie Nano monitors during flights in commercial aircraft; (2) Evaluation of measurements above water bodies. Although most experiments were performed with bGeigie Nano monitors, the results also apply to the CzechRad due to its very similar architecture, although it uses a bit different electronic hardware parts.

### 3.1. Measurements In aircraft

#### 3.1.1. Dose Rate by Altitude

The values measured during the evaluated flights (Table 1) are shown in Figure 3. Results appear essentially consistent between the flights. Dispersion and data noise are still high. Apart from statistical fluctuations, systematic reasons may be: different attenuation by the aircraft shell; radiation of the aircraft, the passengers and other objects; variations in outside air pressure which distort the relationship with altitude; the latitude effect (sec. 2.3.3), since the journeys took place between about 35° N (Heraklion) and 60° N (Bergen). The variation due to the solar cycle is probably low since all flights took place near maximum solar activity. To reduce noise, a 6 point running average was applied, corresponding to  $6 \times 5 \text{ s} = 1/2 \text{ minute}$  average values labelled AM6 is shown in Figure 4 together with a fitted polynomial of order 3. (The fit to the original, non-averaged data is very similar).

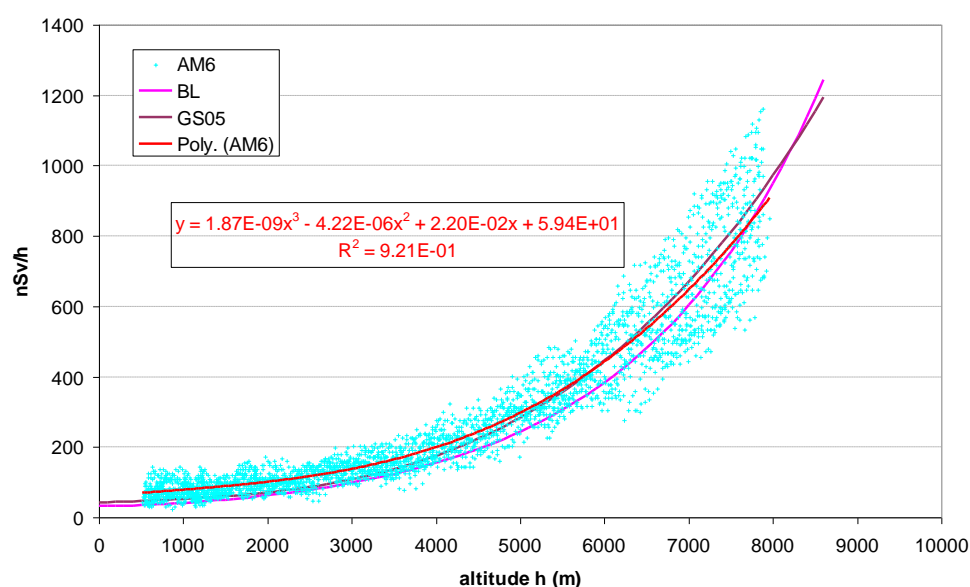


**Figure 4.** All values (30 s running averages) plotted in one graph, and regression curve (polynomial of order 3). Only values measured at least 400 m above ground and below 8000 m used.

The values measured with the bGeigie Nano can be compared with the theoretical values from the Bouville-Lowder formula and the GS05 (eqs. 1 and 2, see sec. 2.3.1) at same altitude. Figure 5 shows a quite good linear correlation with the GS05. The correlation with the values according to BL is worse and visibly non-linear (not shown here; it can well be approximated with a quadratic function). Evidently G-M detectors react to cosmic radiation differently from ionization chambers, although the curves look very similar in the previous figures.

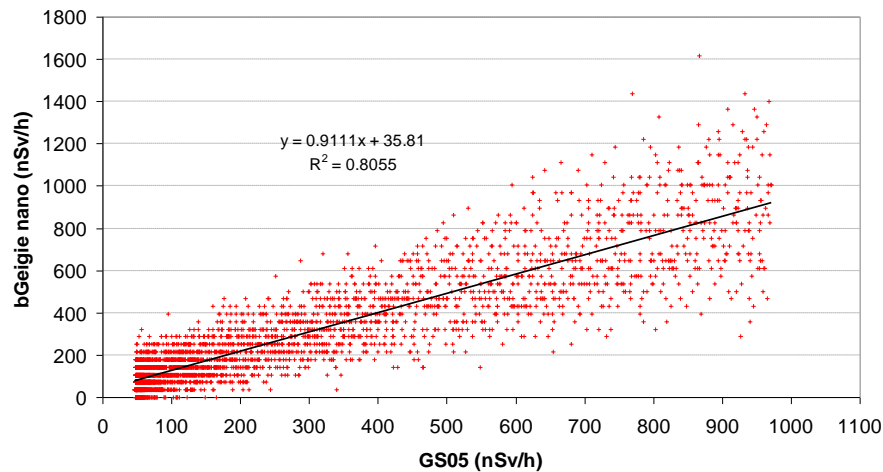


**Figure 5.** Correlation between recorded bGeigie Nano values and theoretical values for a GS05 monitor.

3.1.2. Latitude Effect

From the individual dose rate vs. altitude scatter plots and GPS altitudes, approximate cruising altitudes were identified according to the clusters, Figure 6, summarized in Table 1. Plots of the normalized response  $Y_{norm}$  are shown in Fig 7a, for flight altitudes below 8000 m, corresponding to the ascent and descent phases, and above 10,000 m, corresponding to cruise altitude, in Figure 7b.

The latitude effect is visible in both cases, but more distinct in high altitude > 10 km. The effect is not linear with altitude. Therefore a power model and a second degree polynomial have been fitted. These fits are purely empirical and have no physical rationale. The stronger effect in high altitude can be seen from the higher exponent (power model) and the higher first order term (polynomial model). It would be worthwhile to investigate the effect by altitude in more detail, but the database is not sufficient for this.

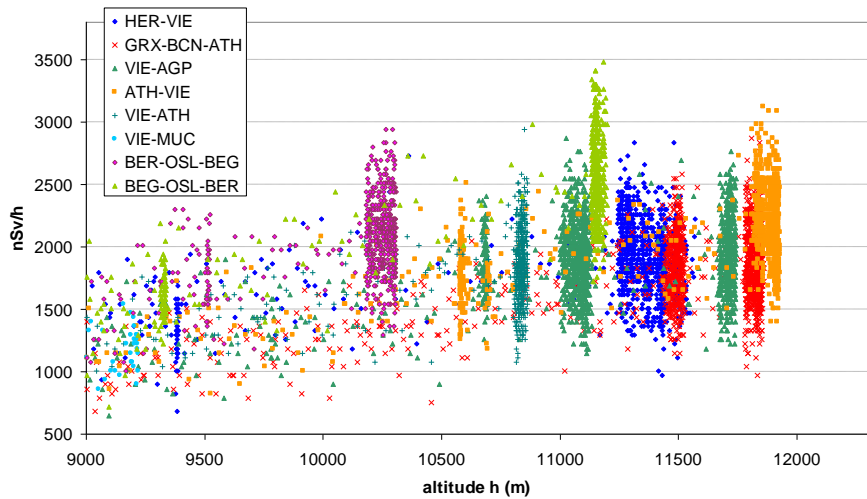


**Figure 6.** Identification of cruising altitude from clusters formed by dose rate data vs. GPS altitude.

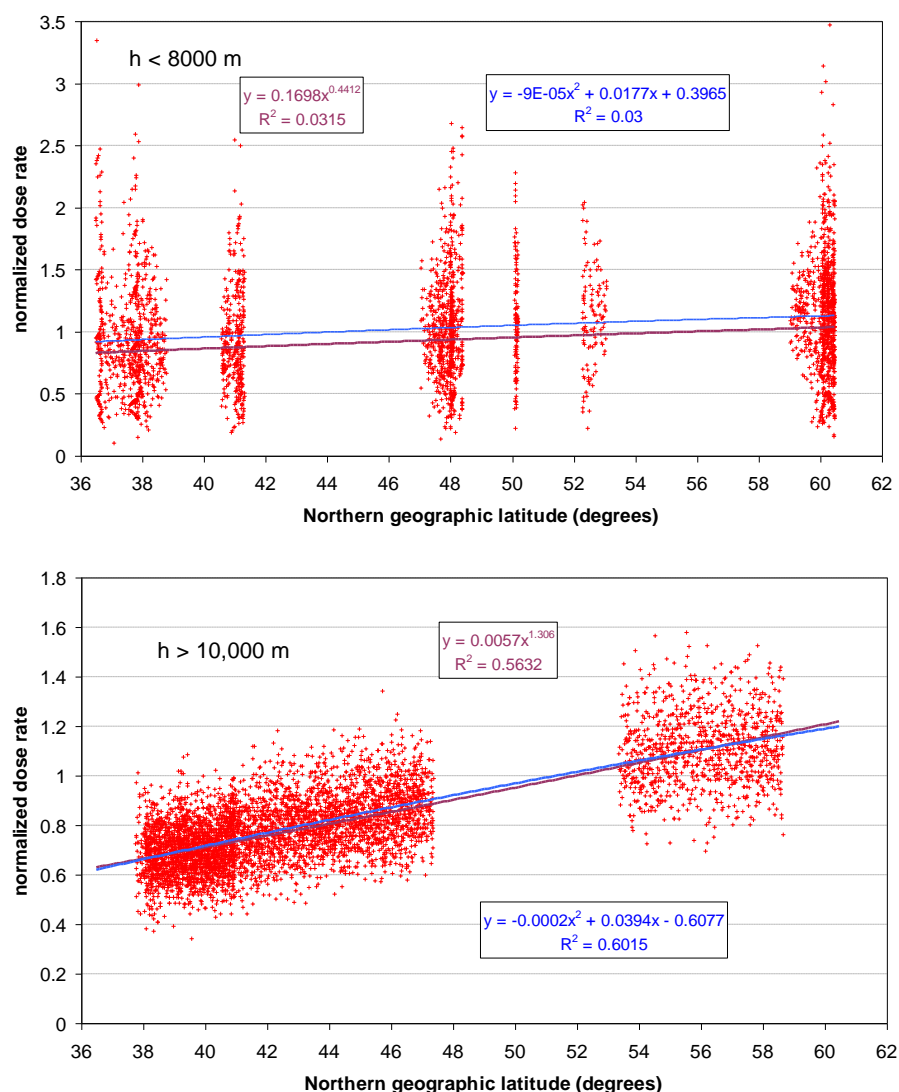


**Figure 7.** Scatter plots of normalized dose rate vs. geographic latitude. (a) Flight altitude < 8000 m, (b) >10,000 m.

### 3.2. Measurements Above Water Bodies

Sources of the data used for the analysis are shown in Table 2 and in more detail in Annex A. Rn contributions are very rough estimates in absence of measured values. An uncertainty of 50% is assumed; it may be even higher. For the equilibrium factor F we set 0.6 and DCF=0.3 (sec. 2.5.3). Other contributions (sec. 2.6.2): very rough guesses, based on the visual assessment of the exposure situation, uncertainty 50% assumed.

The resulting regression plot of standardized measured against theoretical dose rate according to the GS05 monitor following the model given in sec. 2.6.2 is shown in Figure 8. x-axis uncertainty is chosen 10% lacking better knowledge. Detailed results of different regression models performed with Past 4.17 software [69] are given in Table 3.



**Table 2.** Data used for evaluation of lake experiments. Altitude: meters a.s.l; hor / ver: horizontal or vertical orientation of the monitors; Rn contribution: Bq/m³. Other contributions: 1 nSv/h, if not stated otherwise.

Location	altitude (m)	hor / ver	remarks; assumed Rn concentration
Pacific ocean, 2019	1	ver	Rn: 0
Helicopter ascent above Mediterranean, Southern France, 2019	90 - 610	hor	Rn: 0; other: 2; 5 altitude steps, 1 measurement each
Sea off Costa Rica, 2020	1	hor	Rn: 0
Lake Balaton, Hungary, 2020	100	both	Rn: 7; 2 measurements
North Sea off coast, Germany, 2020	3	ver	Rn: 1; 2 measurements
Danube bridge, Vienna, Austria, 2020	172	both	Rn: 7; other: 3; 4 measurements
Danube ferry crossing, near Vienna, 2020	165	ver	Rn: 7
Frozen lake near Prague, Czech Republic. 2021	246	hor	Rn: 10; 4 measurements
Lipno lake, Southern Czech Republic, 2021	726	both	Rn: 15; 22 measurements
Bridge above Hardanger Fjord, Norway, 2022	30	ver	Rn: 5; other: 3; possible interference by adjacent rocks
Bortolan lake, Poços de Caldas, Brazil, 2023	1240	both	Rn: 10; other: 2; 2 measurements
Lhota lake near Prague, Czech Republic, 2024	173	both	Rn: 10; 14 measurements

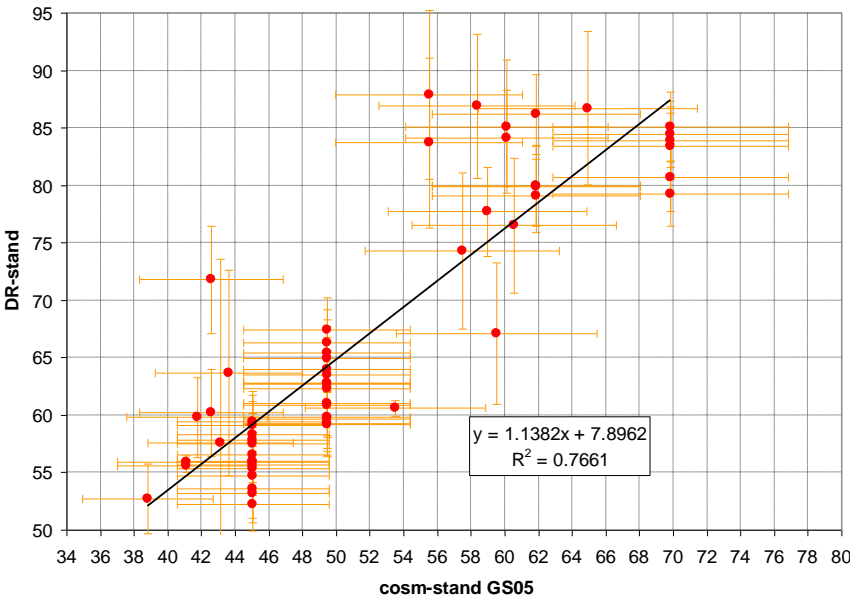


**Figure 8.** Linear regression of the standardized measured dose rate, DR-stand (nSv/h) against standardized theoretical GS05 dose rate (nSv/h).

**Table 3.** Regression results for the linear model standardized bGeigie Nano measurements vs. theoretical results for GS05, eq. 2, and Bouville-Lowder (B-L) formula, eq. 1.

statistic	x = stand. GS05	x = stand. B-L
Ordinary least square:		
intercept	7.90 ± 4.40	7.22 ± 4.16
slope	1.138 ± 0.083	1.538 ± 0.105
Orthogonal (RMA):		
intercept	-0.5 ± 4.4	-0.3 ± 4.2
slope	1.300 ± 0.083	1.731 ± 0.105
r <sup>2</sup> ; p (both):	0.77; 1.2e-19	0.79; 6.8e-21

While correlation is clearly visible, the data points are strongly scattered. Reasons may be wrong estimates of certain input parameters such as Rn concentrations, variation of the latitude factor or variation of parameters between individual devices, for example RResp or the internal BG.

The scatter plot of measured dose rate vs. altitude appears very dispersed, Figure 9. Fitting exponential models with Past4.17 software results in the following parameters:

model  $y = a \exp(bx)$ :  $a = 62.14 \text{ nSv/h}$ ,  $b = 0.000181 \text{ m}^{-1}$ ,  $r^2 = 0.12$  (6a)

model  $y = a \exp(bx) + c$  (shown in Figure 9):  $a = 1.516 \text{ nSv/h}$ ,  $b = 0.002166 \text{ m}^{-1}$ ;  $c = 62.26 \text{ nSv/h}$ ;  $r^2 = 0.13$ ;  $a+c = 63.78 \text{ nSv/h}$ . (6b)

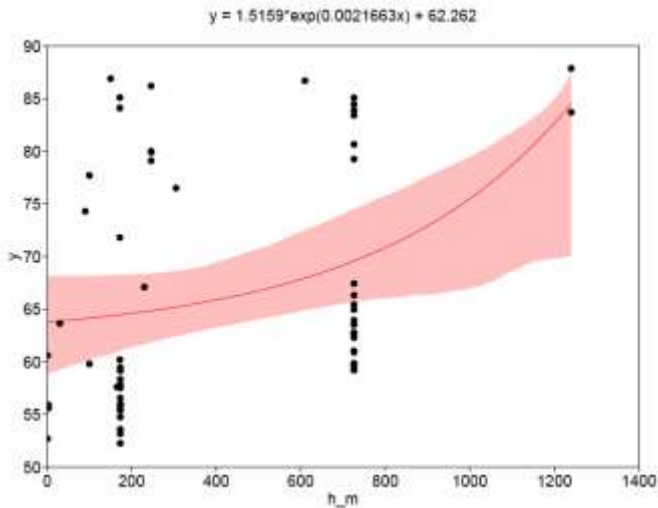


**Figure 9.** Fitted exponential model. x-axis: altitude (m a.s.l.), y-axis: standardized measured dose rate (nSv/h). Shaded area: 95% confidence interval.

4. Conclusions

(1) Essentially, the response of the bGeigie Nano and CzechRad monitors to altitude is as could be expected for G-M detectors. Two types of experiments, which however both rely on measuring in different altitude above sea level, lead to qualitatively similar results.

(2) Different functions of the bGeigie Nano's response to cosmic radiation, estimated from data, are plotted in Figure 10. One can see that for low altitude, models derived from the lake experiments "lake exp 1" (eq. 6a), "lake BL" and "lake GS05" (Table 3) perform similarly, as does the model "airplane poly" (Figure 5). For higher altitude, both models derived from airplane experiments (Figs. 4, 5) perform about equally.

The functions represent means over Northern latitudes typical for Europe. For an approximate latitude correction, one can use the results of Figs. 7. But apparently the latitude effect increases with altitude: our data are not sufficient to evaluate this additional effect.

All results apply to high solar activity. Approximate adjusting could be made using eq. (3). However, it has been derived for low altitude measurements and also in this case we do not know its altitude dependence. (Eq. 3 has been used in the evaluation of the lake experiments, sec. 2.6.2 and 3.2).

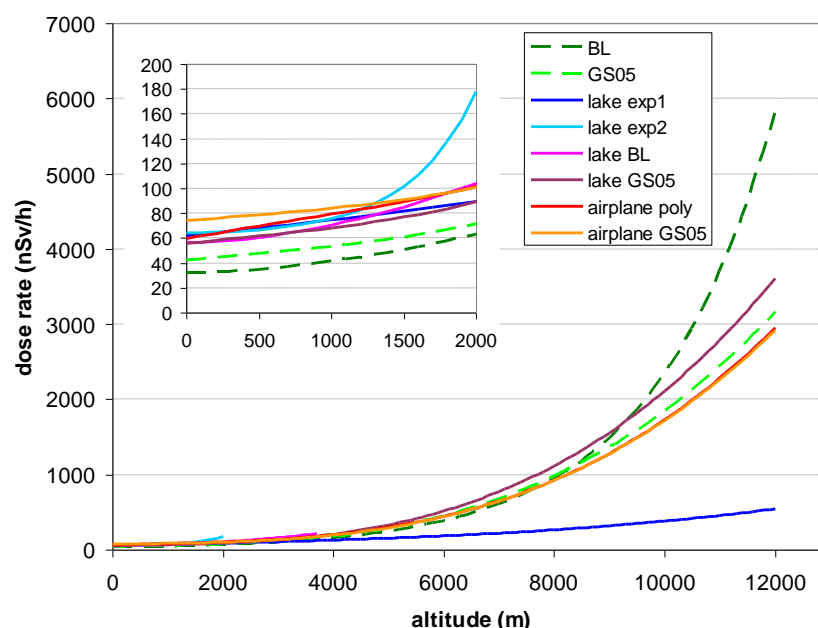


**Figure 10.** Comparison of different models of response of the bGeigie Nano to cosmic radiation. Dashed curves: Bouville-Lowder (BL) formula and GS05 model. BL: eq. (1); GS05: eq. (2); Lake BL, GS05: from table 3; Lake exp1 and lake exp2: models eq. (6a,b); Airplane poly, GS05: Figs. 4 and 5.

(3) A reasonable estimate of the internal background is 10 nSv/h, although variation between individual devices must be expected. Estimation of individual BGs was not possible with the experiments reported here.

We plan to continue these experiments including more exemplars of bGeigie Nano and CzechRad. In particular the anisotropic response of pancake detectors to cosmic radiation (sec. 2.2.1) shall be further investigated. Also a detailed characterization of the CzechRad including a calibration report is planned to be published later.

**Author Contributions:** Conceptualization, methodology and statistical evaluation: PB; Experiments: PK; Text writing, discussion and internal revision: all. All authors have read and agreed to the published version of the manuscript.

**Funding:** This research received no external funding.

**Institutional Review Board Statement:** Not applicable.

**Data Availability Statement:** Some data are available on justified request.

**Conflicts of Interest:** The authors declare no conflicts of interest.

### Acronyms

ADR - Ambient dose rate  
 ADER - Ambient dose equivalent rate  
 AM, SD, SE - arithmetical mean, standard deviation, standard error  
 BG - background  
 CS, CM - Citizen Science, Monitoring  
 G-M counter - Geiger Müller counter  
 QA - Quality Assurance

SCR - Secondary cosmic radiation

## Appendix A

Experiments for determining internal background and cosmic response: some additional information about the experiments mentioned in Table 2, section 3.2.

### *Pacific ocean crossing, 2019*

In a previous paper, [3], the following estimate has been performed (text taken from the paper):

A very approximate preliminary estimate of the internal BG (also called self effect or intrinsic BG) can be gained the following way: A bGeigie Nano detector has been used during crossing the Pacific Ocean. The observed ADER consists of BG + cosmic radiation + some contribution of the structural material of the ship and radiation emitted by people ( $^{40}\text{K}$  mainly). Pictures of the ship and information about the circumstances of the journey can be found in <https://safecast.org/2019/06/lessons-from-a-record-setting-pacific-crossing-with-safecast-on-board/> and <https://safecast.org/2019/01/safecast-on-board-for-blind-sailors-attempt-to-cross-the-pacific-ocean/> . <https://safecast.org/2019/06/lessons-from-a-record-setting-pacific-crossing-with-safecast-on-board/>

Assuming 41.7 nSv/h as ADER on sea level and  $53.7 \pm 12.7$  (1 SD) nSv/h as observed during the ocean crossing, we find a difference of 12 nSv/h. Accounting for a possible contribution of ship and crew, about 1 nSv/h, we assume an internal BG corresponding approximately 11 nSv/h.

### *Off the coast of Costa Rica, 2020*

Measurements on a glass fibre boat off the Pacific coast were performed with a bGeigie nano in horizontal position, the window facing downwards. Again for ADER at sea level + internal BG + possible contribution of boat and persons,  $61.1 \pm 14.5$  nSv/h was found. Location: 8.7° northern latitude, 83.3° western longitude.

### *Tidal area of the North Sea, 2020*

A bGeigie Nano was fixed on a buoy not far from the North Sea shore and dose rate measured during high tide. We assume a Rn concentration of 1 Bq/m<sup>3</sup> close to the shore. Remaining terrestrial radiation and the metal structure on which the monitor was suspended may add 1 nSv/h.

The experiment was performed by Dr Christoph Ilgner, Ministry for Environment, Agriculture and Energy of Saxony-Anhalt State in Magdeburg, Germany. The location is 53.91° northern latitude, 8.67 eastern longitude, near Cuxhaven, Germany.

### *Lake Balaton, Hungary, 2020*

Measurements were performed on a pedal boat made of plastic, rented at the public beach of Balatonalmádi, summer 2020. Measurement location was about 500 m off the shore. However, the lake is quite shallow, probably less than 3 m, so that some residual terrestrial radiation must be expected, for which together with the boat plus passengers we guess 1 nSv/h. The location is 47.03° northern latitude, 18.02° eastern longitude.

### *Measurements from bridges, 2020 and 2022*

In summer 2020, measurements were performed while crossing two bridges over the Danube and the New Danube in Vienna, Nordsteg and Jedleseer Brücke, respectively. The main Danube river is at least 300 m wide which guarantees sufficient distance to the terrestrial environment. The New Danube is a bit less than 200 m wide, so that some terrestrial radiation influence can be expected. The Nordsteg bridge (48.25° northern latitude, 16.38° eastern longitude) is made of concrete, which yields a radiation background due to building material, for which we guess 3 nSv/h. Jedleseer Brücke (48.27° northern latitude, 16.37° eastern longitude) is essentially a steel construction with some asphalt pavement. Its radiation background can be expected low; as a guess, we set 3 nSv/h. Both rivers are >3 m deep, the bridges are about 10 m above water surface. Altitude a.s.l. is 172 m. For Rn concentration, we guess 7 Bq/m<sup>3</sup>.

Two passages in a bus over the Hardangerbrua, a large suspension bridge over the Hardanger Fjord, Norway, in Sept. 2022, were also evaluated. The bridge is over 50 m above water level, the fjord is several 100 m deep. Distance to the shores is sufficient. Radiation by bridge and bus may contribute 3 nSv/h. For Rn we guess 5 Bq/m<sup>3</sup>. The location is 60.40° northern latitude, 5.32° eastern longitude.

*Danube ferry, 2020*

Dose rate was measured during the crossing of the Danube near Vienna on a small wooden passenger / bicycle ferry. The Danube is wide enough and some meters deep. The crossing takes about 15 minutes, but only data from a small section in the middle of the river were used for evaluation. The location is 48.33° northern latitude, 16.33° eastern longitude.

*Frozen lake near Prague, 2021*

A small lake in a park at the outskirts of Prague, location 50.04° northern latitude, 14.54° eastern longitude. Altitude a.s.l. is 246 m. For Rn concentration, we guess 10 Bq/m<sup>3</sup> [70]. For possibly remaining terrestrial and other components, we set 1 nSv/h.

*Helicopter ascent, 2019*

A bGeigie Nano was operated during a helicopter flight above the Mediterranean Sea whose purpose was QA of professional instruments. The experiment was performed at about 43.2° northern latitude, 4.9° eastern longitude. Measured ADR is composed of secondary cosmic radiation, internal background, gamma radiation of the helicopter and personnel and gamma radiation emitted by Rn progeny in the air.

Measurements were performed in 300, 500, 750, 1000, 2000 feet above sea level, or about 90, 150, 230, 305 and 610 m. The detector was positioned horizontal (axis vertical) with window facing downwards. The results shown here are based on 64 to 69 measurement cycles à 5 s in each altitude. As Figure A1 shows, the differences between altitudes are very small, which is no surprise since altitude variation is also small. To estimate response at sea level, regression was performed for a linear and exponential model; the approximation is fair for small altitude difference. Both models yield an intercept 2.07, with SE 0.18 for the linear model. The slope (5.5 e-4 (counts/5s per m) for the linear model) is not significantly greater than zero. With calibration 334 cpm/( Sv/h) one finds 74.4 nSv/h for sea level. – However, feeding the data into the more comprehensive model shown in section 2.2 leads to more reliable results. No relevant dose rate due to Rn is expected in this case. As the remaining component (helicopter body, persons), we set 2 nSv/h.

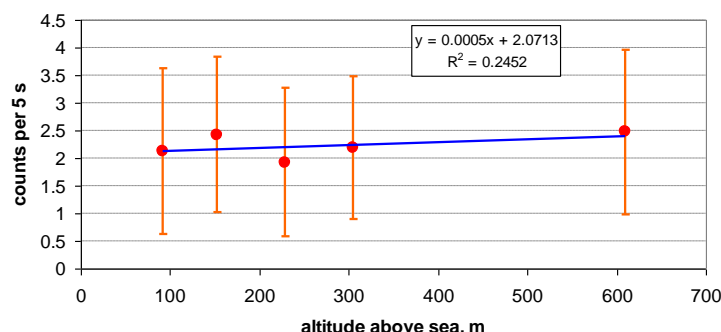


**Figure A1.** bGeigie readings in a helicopter in different altitude. Arithmetical mean and standard deviations.

*Lake Lipno in S Bohemia, summer 2021*

Two sets of bGeigie Nano monitors (two boxes containing 8 and 4 units) were used for measurements in a site with about 8 m water depth and >500 m distance from the shore. Measurements with vertical and horizontal orientations of the detectors were performed. One monitor failed, so that there are (8+4-1)×2=22 measurements. The location is 48.7° northern latitude, 17.1° eastern longitude, 726 m a.s.l.

*Lake Lhota, near Prague, Czech Republic, autumn 2024*

On lake Lhota near Prague, several bGeigie Nano and Czechrad monitors were exposed on a raft away from the shore in vertical and horizontal position. The main purpose was examination of the difference between vertical and horizontal orientations of the monitors. Details of the experiments will be published elsewhere. Counting times about 30 minutes. The location is 50.27° northern latitude, 14.67° eastern longitude, altitude = 173 m a.s.l.

*Lake Bortolan, Poços de Caldas, Brazil, November 2023*



A similar experiment has been performed using two bGeigie Nano on the lake Represa Bortolan near as part of a radiometric exercise, November 2023 [71]. The location is 21.79° southern latitude, 46.64° western longitude, 1240 m a.s.l. In this case, the carrier was a rented pedal boat. Counting times were between 6 and 12 minutes only, which results in higher uncertainty than for the Lhota lake experiment, although on the other hand, the higher altitude means higher count rate.

## References

1. Vohland, K.; Landzandstra, A.; Ceccaroni, L.; Lemmens, R.; Perelló, J.; Ponti, M.; Samson, R.; Wagenknecht, K.; (eds.) The Science of Citizen Science. 2021, Springer International Publishing, DOI 10.1007/978-3-030-58278-4, [www.springer.com/gp/book/9783030582777](http://www.springer.com/gp/book/9783030582777) (open access; accessed 14 August 2021)
2. Brown, A.; Franken, P.; Bonner, S.; Dolezal, N.; Moross, J. Safecast: successful citizen-science for radiation measurement and communication after Fukushima. *Journal of Radiological Protection* **2016**, 36 (2), S82 – S101; doi:10.1088/0952-4746/36/2/s82
3. Bossew, P.; Kuča, P.; Helebrant, J. Mean ambient dose rate in various cities, inferred from Safecast data. *Journal of Environmental Radioactivity* **2020**, 225, 106363; <https://doi.org/10.1016/j.jenvrad.2020.106363>
4. Bossew, P.; Kuča, P.; Helebrant, J. (2022) Citizen monitoring of ambient dose rate: metrological challenges. Pres., RAD - 10th International Conference on Radiation in Various Fields of Research, Herceg Novi (Montenegro), 13 – 17 June 2022, <http://www.rad2022-spring.rad-conference.org/>
5. Bossew, P.; Kuča, P.; Helebrant, J. (2022) True and spurious anomalies in ambient dose rate monitoring. Pres., ICHLERA, 10th International Conference on High Level Environmental Radiation Areas, Strasbourg (France), 27 – 30 June 2022; <https://indico.in2p3.fr/event/19295/>
6. Kuča, P.; Helebrant, J.; and Bossew, P. (2021) Safecast – a Citizen Science initiative for ambient dose rate mapping; Quality assurance issues., EGU General Assembly 2021, online, 19–30 Apr 2021, EGU21-1343, <https://doi.org/10.5194/egusphere-egu21-1343>, 2021.
7. Kuča, P.; Helebrant, J.; Bossew, P. (2021) Safecast – Citizen Science for radiation monitoring. RAP CONFERENCE PROCEEDINGS, VOL. 6, PP. 32–38, 2021; DOI: 10.37392/RAPPROC.2021.07; <https://www.rap-proceedings.org/papers/RapProc.2021.07.pdf>
8. Kuča, P.; Helebrant, J.; Bossew, P. (2022) Characterization of the bGeigie Nano instrument used in Citizen Science dose rate monitoring. Pres., RAP - International Conference on Radiation Applications, Thessaloniki (Greece), 6-10 June 2022, <https://www.rap-conference.org/22/>
9. Kuča, P.; Helebrant, J.; Bossew, P. (2022): Citizen monitoring of ambient dose rate: The Safecast project. Pres., IRPA - 6th European Congress on Radiation Protection, 30.5. - 3.6.2022 Budapest (Hungary)
10. UNSCEAR: United Nations Scientific Committee on the Effects of Atomic Radiation Reports to the General Assembly, with Annexes. All reports: <https://www.unscear.org/unscear/en/publications/scientific-reports.html> (accessed 10 Nov 2022)
11. O'Brien, K.; Friedberg, W.; Sauer, H. H.; Smart, D. F. Atmospheric cosmic rays and solar energetic particles at aircraft altitudes. *Environment International* **1996**, 22, 9–44. doi:10.1016/s0160-4120(96)00086-4
12. Wissmann, F. Variations observed in environmental radiation at ground level. *Radiation Protection Dosimetry* **2006**, 118 (1), 3–10, <https://doi.org/10.1093/rpd/nci317>
13. Spurný, F. Radiation doses at high altitudes and during space flights. *Radiation Physics and Chemistry* **2000**, 61(3-6), 301–307. doi:10.1016/s0969-806x(01)00253-5
14. Bouville, A.; Lowder, W.M. Human population exposure to cosmic radiation. *Radiat. Prot. Dosim.* **1998**, 24 (1-4), 293-299. <https://doi.org/10.1093/oxfordjournals.rpd.a080290>
15. Lowder, W.M.; O'Brien, K. (1972): Cosmic-ray dose rates in the atmosphere. Health and Safety Laboratory, U.S. Atomic Energy Commission, HASL-254 report.
16. SpaceWeather (2022): Solar Cycle progression. <https://www.spaceweatherlive.com/en/solar-activity/solar-cycle.html>
17. Wissmann, F.; Dangendorf, V.; Schrewe, U. Radiation exposure at ground level by secondary cosmic radiation. *Radiation Measurements* **2005**, 39 (1), 95 – 104. DOI: 10.1016/j.radmeas.2004.03.025
18. Wissmann, F.; Rupp, A.; Stöhlker, U. Characterization of dose rate instruments for environmental radiation monitoring. *Kerntechnik* **2007**, 72 (4), 193 – 198; <https://doi.org/10.3139/124.100341>
19. Cinelli, G.; Bossew, P.; Hernández-Ceballos, M.A.; Tollefsen, T.; De Cort M. (2017): Long-term variation of cosmic dose rate. Presentation, ENVIRA (4th Intl. Conf. on Environmental Radioactivity), Vilnius, Lithuania, 29 May – 2 June 2017; Abstract in Book of Abstracts, p.124, <http://envira2017.ftmc.lt/abstracts.php>. Pres. available from the author.
20. EC (2020): European Commission, Joint Research Centre – Cinelli, G., De Cort, M. & Tollefsen, T. (Eds.), European Atlas of Natural Radiation, Publication Office of the European Union, Luxembourg, 2019. Printed version: ISBN 978-92-76-08259-0; doi:10.2760/520053; Catalogue number KJ-02-19-425-EN-C; Online version: ISBN 978-92-76-08258-3; doi:10.2760/46388 ; Catalogue number KJ-02-19-425-EN-N; <https://remon.jrc.ec.europa.eu/About/Atlas-of-Natural-Radiation/Download-page>

21. Sato T. (2001): Evaluation of World Population-Weighted Effective Dose due to Cosmic Ray Exposure. *Scientific Reports* **2000**, 6, 33932; DOI: 10.1038/srep33932
22. ICRU (2010): ICRU Report 84, Reference Data for the Validation of Doses from Cosmic-Radiation Exposure of Aircraft Crew. *Journal of the ICRU* 10 (2); <https://journals.sagepub.com/toc/crua/10/2>
23. Bossew, P.; Cinelli, G.; Hernández-Ceballos, M.; Cernohlawek, N.; Gruber, V.; Dehandschutter, B.; Menneson, F.; Bleher, M.; Stöhlker, U.; Hellmann, I.; Weiler, F.; Tollefsen, T.; Tognoli, P.V.; de Cort M. Estimating the terrestrial gamma dose rate by decomposition of the ambient dose equivalent rate. *J. Environmental Radioactivity* **2017**, 166, 296 - 308, <http://dx.doi.org/10.1016/j.jenvrad.2016.02.013>
24. Spiers, F.W.; Gibson, J.A.B.; Thompson, I.M.G. (1981) A guide to the measurement of environmental gamma-ray dose rate. British Committee on Radiation Units and Measurements. <http://cds.cern.ch/record/1057200/files/CM-P00066948.pdf> (accessed 22 July 2020)
25. Lewis, V. E.; Hunt, J. B. Fast neutron sensitivities of Geiger-Mueller counter gamma dosimeters. *Physics in Medicine and Biology* **1978**, 23(5), 888–893. doi:10.1088/0031-9155/23/5/005
26. Guldbakke, S.; Jahr, R.; Lesiecki, H.; Schölermann, H. (1980): Neutron sensitivity of Geiger-Müller photon dosimeters for neutron energies between 100 keV and 19 MeV. [https://www.irpa.net/irpa5/cdrom/VOL.2/J2\\_37.PDF](https://www.irpa.net/irpa5/cdrom/VOL.2/J2_37.PDF)
27. Mijneer, B. J.; Guldbakke, S.; Lewis, V. E.; Broerse, J. J. Comparison of the fast-neutron sensitivity of a Geiger-Mueller counter using different techniques. *Physics in Medicine and Biology* **1982**, 27(1), 91–96. doi:10.1088/0031-9155/27/1/009
28. Maughan, R. L.; Yudelev, M.; Kota, C. A measurement of the fast-neutron sensitivity of a Geiger - Müller detector in the pulsed neutron beam from a superconducting cyclotron. *Physics in Medicine and Biology* **1996**, 41(8), 1341–1351. doi:10.1088/0031-9155/41/8/007
29. Nakamura, T. Cosmic-ray Neutron Spectrometry and Dosimetry. *Journal of Nuclear Science and Technology* **2008**, 45:sup5, 1-7, DOI: 10.1080/00223131.2008.10875772
30. Lowder, W. M.; Beck, H. L. Cosmic-ray ionization in the lower atmosphere. *Journal of Geophysical Research* **1966**, 71(19), 4661–4668. doi:10.1029/jz071i019p04661
31. Cinelli, G.; Gruber, V.; De Felice, L.; Bossew, P.; Hernandez-Ceballos, M.A.; Tollefsen, T.; Mundigl, S.; De Cort M. European annual cosmic-ray dose: estimation of population exposure. *J. of Maps* **2017**, 13 (2), 812 – 521; <http://dx.doi.org/10.1080/17445647.2017.1384934>
32. Hernández-Ceballos, M.A.; Cinelli, G.; Marín Ferrer, M.; Tollefsen, T.; De Felice, L.; Nweke, E.; Tognoli, P.V.; Vanzo, S.; De Cort, M. A climatology of <sup>7</sup>Be in surface air in European Union. *J. Environ. Radioactivity* **2015**, 141, 62-70, doi:10.1016/j.jenvrad.2014.12.003
33. BGS (British Geological Survey; n.y.): The Earth's Magnetic Field: An Overview. <https://geomag.bgs.ac.uk/education/earthmag.html> ; geomagnetic coordinate calculator: [https://geomag.bgs.ac.uk/data\\_service/models\\_compass/coord\\_calc.html](https://geomag.bgs.ac.uk/data_service/models_compass/coord_calc.html) (accessed 25 Oct 2024)
34. World Data Center for Geomagnetism, Data Analysis Center for Geomagnetism and Space Magnetism, Graduate School of Science, Kyoto University Kyoto: <https://wdc.kugi.kyoto-u.ac.jp/igrf/gggm/> (accessed 25 Oct 2024)
35. Hůlka, J.; Kuča, P.; Helebrant, J.; Rozlívka, Z. (2017): Citizens Measurements in Radiation Protection and Emergency Preparedness and Response - its role, pros and cons. Pres., EUROSAFE 2017; [https://www.eurosafe-forum.org/sites/default/files/Eurosafe2017/Seminars/4\\_08\\_Presentation\\_Kuca\\_final\\_ppt.pdf](https://www.eurosafe-forum.org/sites/default/files/Eurosafe2017/Seminars/4_08_Presentation_Kuca_final_ppt.pdf) (acc. 26 Jan 2019)
36. Kuča, P.; Helebrant, J.; Hůlka J. (2017) Role of citizens measurements in radiation protection, emergency preparedness and response - its pros and cons. ICRP 4th International Symposium on the System of Radiological Protection & 2nd European Radiological Protection Week, October 10-12 2017, Paris, France. [http://www.icrp-erpw2017.com/upload/presentations/ERPW%20Communication/Session\\_02/Session%2002\\_5\\_KUCA\\_Presentation.pdf](http://www.icrp-erpw2017.com/upload/presentations/ERPW%20Communication/Session_02/Session%2002_5_KUCA_Presentation.pdf) (acc. 26 Jan 2019)
37. Helebrant, J.; Kuča, P.; Hůlka, J. (2018) RAMESIS :Radiální měřicí síť pro instituce a školy k zajištění včasné informovanosti a zvýšení bezpečnosti občanů měst a obcí. (In Czech); <https://www.suro.cz/cz/vyzkum/vysledky/safecast/09Hulka.pdf> (acc 26 Jan 2019)
38. SÚRO (2019) Detektor záření SAFECAS T a jeho využití pro veřejnost. (In Czech); <https://www.suro.cz/cz/vyzkum/vysledky/safecast> (acc. 26 Jan 2019)
39. QGIS - A Free and Open Source Geographic Information System, <https://www.qgis.org/en/site/>
40. Vanek, M.; Ďuríková, A.; Salva, J. (2018) Safecast bGeigie Nano as a tool for teaching students to understand monitoring environmental radioactivity. Proc., Conference: Earth in a Trap? 2018, Analytical Methods in Fire and Environmental Science, Hodruša-Hámre, Slovak Republic; [https://www.researchgate.net/publication/326031794\\_Safecast\\_bGeigie\\_Nano\\_as\\_a\\_tool\\_for\\_teaching\\_students\\_to\\_understand\\_monitoring\\_environmental\\_radioactivity](https://www.researchgate.net/publication/326031794_Safecast_bGeigie_Nano_as_a_tool_for_teaching_students_to_understand_monitoring_environmental_radioactivity) (acc. 26 Jan 2019)

41. CzechRad (2021) Mobile detector for radiation mapping - similar to SAFECAST bGeigie Nano. <https://github.com/juhele/CzechRad> (accessed 20 Feb 2021)
42. Yogeshwar R. (2014) Calibration of SAFECAST bGeigie-nano – Radiation Detector (# 1025). Document supplied to one of the authors (PB) by Safecast.
43. Wagner, E.; Sorom, R.; Wiles, L. Radiation monitoring for the masses. *Health Physics* **2016**, *110* (1), 37 – 44; DOI: 10.1097/HP.0000000000000407
44. Tanji, T.; Okino, M.; Sugioka, I.; Mochizuki, S. Radon and its Daughters in the Atmosphere Over the Equatorial Pacific Ocean. *Radiation Protection Dosimetry* **1992**, *45* (1-4), 399–401, <https://doi.org/10.1093/rpd/45.1-4.399>
45. Čeliković, I.; Pantelić, G.; Vukanac, I.; Krneta Nikolić, J.; Živanović, M.; Cinelli, G.; Gruber, V.; Baumann, S.; Quindos Poncela, L.S.; Rabago, D. Outdoor Radon as a Tool to Estimate Radon Priority Areas—A Literature Overview. *Int. J. Environ. Res. Public Health* **2022**, *19*, 662. <https://doi.org/10.3390/ijerph19020662>
46. ICRP, 2020. Dose coefficients for external exposures to environmental sources. ICRP Publication 144. Ann. ICRP 49(2). <https://journals.sagepub.com/doi/pdf/10.1177/0146645320906277>
47. EPA (2019): External exposure to radionuclides in air, water and soil – Federal guidance report No. 5; EPA 402-R-19-002; [https://www.epa.gov/sites/default/files/2019-08/documents/fgr\\_15\\_final\\_508\\_2019aug02.pdf](https://www.epa.gov/sites/default/files/2019-08/documents/fgr_15_final_508_2019aug02.pdf)
48. Smetsers, R. C. G. M.; Blaauboer, R. O. A Dynamic Compensation Method for Natural Ambient Dose Rate Based on 6 Years Data from the Dutch Radioactivity Monitoring Network. *Radiation Protection Dosimetry* **1997**, *69*(1), 19–31. doi:10.1093/oxfordjournals.rpd.a031883
49. DOE (1988): External Dose-Rate Conversion Factors for Calculation of Dose to the Public. DOE/EH—0070. <https://www.osti.gov/servlets/purl/6953527>
50. Kocher D.C. (1981): Dose rate conversion factors for external exposure to photons and electrons. NUREG/CR-1918; [https://digital.library.unt.edu/ark:/67531/metadc1058696/m2/1/high\\_res\\_d/5020464.pdf](https://digital.library.unt.edu/ark:/67531/metadc1058696/m2/1/high_res_d/5020464.pdf)
51. Kümmel, M.; Dushe, C.; Müller, S.; Gehrcke, K. Outdoor <sup>222</sup>Rn-concentrations in Germany - part 1 - natural background. *J. Environ. Radioact.* **2014**, *132*, 123-130. <https://doi.org/10.1016/j.jenvrad.2014.01.012>
52. Chen, J.; Harley, N. H. A Review of Indoor and Outdoor Radon Equilibrium Factors—part I. *Health Physics* **2018**, *115*(4), 490–499. doi:10.1097/hp.0000000000000909
53. Cuculeanu, V.; Sonoc, C.; Georgescu, M. Radioactivity of Radon and Thoron Daughters in Romania. *Radiation Protection Dosimetry* **1992**, *45* (1-4), 83-485. DOI: 10.1093/oxfordjournals.rpd.a081586
54. Kataoka, T.; Tsukamoto, O.; Yunoki, E.; Michihiro, K.; Sugiyama, H.; Shimizu, M.; Mori, T.; Sahashi, T.; Fujii, S. Variation of <sup>222</sup>Rn Concentration in Outdoor Air due to Variation of the Atmospheric Boundary Layer. *Radiation Protection Dosimetry* **1992**, *45* (1-4), 403–406, <https://doi.org/10.1093/rpd/45.1-4.403>
55. Dueñas, C.; Pérez, M.; Fernández, M.C.; Carretero, J. Radon concentrations in surface air and vertical atmospheric stability of the lower atmosphere. *Journal of Environmental Radioactivity* **1996**, *31* (1), 87 – 102. [https://doi.org/10.1016/0265-931X\(95\)00058-I](https://doi.org/10.1016/0265-931X(95)00058-I)
56. Levin, I.; Born, M.; Cuntz, M.; Langendörfer, U.; Mantsch, S.; Naegler, T.; Schmidt, M.; Varlagin, A.; Verclas, S.; Wagenbach, D. Observations of atmospheric variability and soil exhalation rate of radon-222 at a Russian forest site Technical approach and deployment for boundary layer studies. *Tellus* **2002**, *54B*, 462–475. <https://doi.org/10.1034/j.1600-0889.2002.01346.x>
57. Oikawa, Sh.; Kanno, N.; Sanada, T.; Ohashi, N.; Uesugi, M.; Sato, K.; Abukawa, J.; Higuchi, H. A nationwide survey of outdoor radon concentration in Japan. *Journal of Environmental Radioactivity* **2003**, *65*, 203–213. doi:10.1016/S0265-931X(02)00097-8
58. Sesana, L.; Ottobriani, B.; Polla, G.; Facchini, U. <sup>222</sup>Rn as indicator of atmospheric turbulence: measurements at Lake Maggiore and on the pre-Alps. *J. Environmental Radioactivity* **2005**, *86* (2), 271-88; DOI: 10.1016/j.jenvrad.2005.09.005
59. Desideri, D.; Roselli, C.; Feduzi, L.; Assunta Meli, M. Monitoring the atmospheric stability by using radon concentration measurements: A study in a Central Italy site. *Journal of Radioanalytical and Nuclear Chemistry* **2006**, *270*(3), 523–530. doi:10.1007/s10967-006-0458-1
60. Garbero, V.; Dellacasa, G.; Bianchi, D.; Magnoni, M.; Erbetta L. Outdoor radon concentration measurements: some correlation with major urban pollutants. *Radiation Protection Dosimetry* **2009**, *137* (3–4), 332–335. doi:10.1093/rpd/ncp253
61. Omori, Y.; Tohbo, I.; Nagahama, H.; Ishikawa, Y.; Takahashi, M.; Sato, H.; Sekine, T. Variation of atmospheric radon concentration with bimodal seasonality. *Radiation Measurements* **2009**, *44* (9-10), 1045-1050. <https://doi.org/10.1016/j.radmeas.2009.10.077>
62. Liang Zhang , Liguang Zhang and Qiuju Guo A long-term investigation of the atmospheric radon concentration in Beijing, China. *J. Radiol. Prot.* **2009**, *29*, 263–268 doi:10.1088/0952-4746/29/2/012
63. Liang Zhang and Qiuju Guo Observation and analysis of atmospheric radon in Qingdao, China. *J. Radiol. Prot.* **2011**, *31*, 129–134. doi:10.1088/0952-4746/31/1/009
64. Müllerová, M.; Holý, K.; Bulko, M. Results of outdoor radon monitoring in Bratislava and Nováky. *Radiation Protection Dosimetry* **2011**, *145* (2–3), 325–328. doi:10.1093/rpd/ncr068

65. Weller, R.; Levin, I.; Schmithüsen, D.; Nachbar, M.; Asseng, J.; Wagenbach, D. On the variability of atmospheric  $^{222}\text{Rn}$  activity concentrations measured at Neumayer, coastal Antarctica. *Atmos. Chem. Phys. Discuss.* **2013**, *13*, 32817–32847, 2013. [www.atmos-chem-phys-discuss.net/13/32817/2013/](http://www.atmos-chem-phys-discuss.net/13/32817/2013/)
66. Hayashi, K.; Yasuoka, Y.; Nagahama, H.; Muto, J.; Ishikawa, T.; Omori, Y.; Suzuki, T.; Homma, Y.; Mukai, T. Normal seasonal variations for atmospheric radon concentration: a sinusoidal model. *Journal of Environmental Radioactivity*, **2015** *139*, 149–153. <http://dx.doi.org/10.1016/j.jenvrad.2014.10.007>
67. Holý, K.; Müllerová, M.; Bulko, M.; Holá, O.; Melicherová, T. Outdoor  $^{222}\text{Rn}$  behaviour in different areas of Slovakia. *NUKLEONIKA* **2016**, *61* (3), 281 – 288. doi: 10.1515/nuka-2016-0047
68. Bossew, P.; Benà, E.; Chambers, S.; Janik, M. Analysis of outdoor and indoor radon concentration time series recorded with RadonEye monitors. Submitted to *Atmosphere*.
69. Hammer, Ø.; Harper, D.A.T.; Ryan, P.D. PAST: Paleontological statistics software package for education and data analysis. *Palaeontologia Electronica* **2001**, *4*(1): 9pp. [http://palaeo-electronica.org/2001\\_1/past/issue1\\_01.htm](http://palaeo-electronica.org/2001_1/past/issue1_01.htm) Download from <https://www.nhm.uio.no/english/research/resources/past/> (accessed 2.8.2024).
70. Jilek, K.; Slezáková, M.; Thomas, J. Diurnal and seasonal variability of outdoor radon concentration in the area of the NRPI Prague. *Rad. Prot. Dosimetry* **2014**, *160* (1-3), 57 – 61. doi:10.1093/rpd/ncu091
71. Bossew, P.; Da Silva, N.; Alberti, H.; Silva, M.A.; Navarro, F.C.; De Oliveira, T.A.; Cardoso Takahashi, L.; de Souza Filho, O.A.; Otero, U.; Kuča, P.; Helebrant, J. A remarkable small local natural radiation anomaly in Poços de Caldas, Brazil. Subm., *Eur. Phys. J. Special Topics*.

**Disclaimer/Publisher's Note:** The statements, opinions and data contained in all publications are solely those of the individual author(s) and contributor(s) and not of MDPI and/or the editor(s). MDPI and/or the editor(s) disclaim responsibility for any injury to people or property resulting from any ideas, methods, instructions or products referred to in the content.